The ONIX model: a parameter-free multiscale framework for the prediction of self-desiccation in concrete

M. Pathirage[1], D.P. Bentz[2], G. Di Luzio[3], E. Masoero[4], G. Cusatis[1,*]

Abstract

The traditional approach for predicting self-desiccation is to simulate hygro-mechanics directly at the macroscale and to provide hydration-related inputs via phenomenological constitutive models. This manuscript presents instead a novel method that consists of obtaining inputs to such constitutive relations from direct simulations of cement hydration at the microscale, using a state-of-the-art simulator, namely the Cement Hydration in Three Dimensions (CEMHYD3D). This allows avoiding lengthy calibrations from experimental data. The prediction capabilities of the proposed model are demonstrated using experimental data of self-desiccation relevant to about 50 different mix designs of concrete, mortar and cement paste, with water to cement ratios ranging from 0.20 to 0.68 and silica fume to cement ratios from 0.0 to 0.39. The mixes are characterized by various cement chemical compositions, particle size distributions and Blaine finenesses, and the experiments span numerous time scales, from one week up to two years.

Keywords: Self-desiccation, Hydration, ONIX model, CEMHYD3D model, Hygro-Thermo-Chemical model, Multiscale modeling

[☆]Department of Civil and Environmental Engineering, McCormick School of Engineering and Applied Science Northwestern University, Evanston, IL, USA.

[☆☆]Engineering Laboratory National Institute of Standards and Technology, Gaithersburg, MD, USA.(retired)

Department of Civil and Environmental Engineering Politecnico di Milano, Milano, Italy.

School of Civil Engineering and Geosciences Newcastle University, Newcastle upon Tyne, United Kingdom.

[*]Corresponding author's full postal address:Department of Civil and Environmental Engineering, Mc-

1. Introduction

High and Ultra-High Performance Concrete (HPC and UHPC) are amongst the recent breakthrough technologies in civil engineering. These materials have improved concrete durability in aggressive environments, and enabled the construction of complex and long-term cost-effective structures. However, these materials typically undergo self-desiccation to a significantly greater extent compared to ordinary concrete. This is due to their intrinsic mix proportions, i.e. low water to cement ratios, finer cements and addition of supplementary cementitious admixtures such as silica fume.

The term self-desiccation designates the drop of internal relative humidity due to the partial desaturation of pores in a hydrating concrete paste. The initial water to cement ratio, the distribution of unhydrated cement particles and cement hydration chemical reactions and kinetics play a major role in self-desiccation, to cite just a few key factors. While self-desiccation may be beneficial to some extent, e.g. by enhancing resistance to internal frost damage or in concrete flooring applications, it is one of the main causes of early-age cracking, along with thermal stresses (Persson et al., 2005).

Extensive work on modeling and predicting self-desiccation and cement hydration in general has been performed over the years. Available models can be mainly distinguished in two categories: theoretical and/or empirical formulations and direct microstructure development models.

The first category encompasses mostly macroscale models. Although dedicated to the analysis of self-desiccation (Hua et al., 1995; Persson, 1997; Nilsson and Mjörnell, 2005; Chen et al., 2013), most of the models in the literature describe cement hydration processes, in conjunction with hygral-thermal and mechanical considerations. Among them, it is worth citing the dispersion model of Knudsen (1982) and the work of Bentz (2006c) with simple

Cormick School of Engineering and Applied Science, Northwestern University, Tech Building Room A134, 2145 N Sheridan Rd, Evanston, IL 60208-3109.
Corresponding author's email: g-cusatis@northwestern.edu

formulations for hydration based on spatial considerations, as well as the models of Ulm and Coussy (1995) and De Schutter and Taerwe (1996) that describe cement hydration based on reaction kinetics and allow the evaluation of strength in time. In addition, Cervera et al. (1999) proposed a simple model that can take into account the effect of temperature on strength evolution. More complex models allow the description of hydration, heat and moisture flow processes, chemical shrinkage and self-desiccation (Gawin et al., 2006a,b; Lin and Meyer, 2009; Rahimi-Aghdam et al., 2017; Pan et al., 2017; Rahimi-Aghdam and Bažant, 2018). Among them, the Hygro-Thermo-Chemical (HTC) model proposed by Di Luzio and Cusatis (2009a,b) formulates the evolution of cement hydration and of pore relative humidity in concrete based on moisture transport and heat transfer governing equations. The model uses phenomenological evolution laws to describe the reaction degrees for cement and silica fume, and the associated changes in evaporable and chemically bound waters, along with adsorption/desorption isotherms and permeability of concrete. The capability of the HTC model has been demonstrated through extensive numerical studies by many authors (Di Luzio and Cusatis, 2009b; de Freitas et al., 2015; Boumakis et al., 2015; Bocciarelli and Ranzi, 2018a,b; Pathirage et al., 2017). The HTC model is adopted in this study as the macroscale model, which contains several material parameters to be identified.

The second category of models is based on a detailed account of the actual microstructure of cement paste and concrete. This approach reproduces directly the most important microscale phenomena. The first model of this kind was proposed by Jennings and Johnson (1986). This model explicitly simulates cement grains and their Particle Size Distribution (PSD) as a set of spherical entities composed only of tricalcium silicate $(CaO)_3(SiO_2) = C_3S$. Reaction occurs with calcium-silicate-hydrate $(CaO)_{1.7}(SiO_2)(H_2O)_4$ = C-S-H forming on and surrounding the C_3S particles. Navi and Pignat (1996) proposed a similar model that simulates C_3S spherical particles. However, more elaborate processes such as transport phenomena are not taken into account. The Durability Concrete Model (DuCOM) model

(Maekawa et al., 1999) considers heat generation, mass transport and microstructure formation, tackling also the typical overlapping issue of hydrating cement particles, but it is limited by the fact that the cement particles are assumed to have the same composition and to be mono-size. The HymoStruc model (Van Breugel, 1995; Koenders and Van Breugel, 1997; Ye et al., 2003) introduces multiple cement grains within the same volume, with each grain reacting similarly to what was originally proposed by Jennings and Johnson (1986). Overlapping between growing and potentially overlapping C-S-H domains is accounted for in order to respect the volume balance of the reactions, namely conversion of C_3S and water into C-S-H and calcium hydroxide $(CaO)(H_2O)$ = CH. Bishnoi and Scrivener (2009) proposed the µic model, which is similar to the HymoStruc model but does not constrain the C-S-H to grow as circular domains surrounding the C_3S particles. Instead, C-S-H compact hemispherical and needle-like morphologies are included. A distinct model from the aforementioned ones is the Cement Hydration in Three Dimensions (CEMHYD3D) model that was developed at the National Institute of Standards and Technology (NIST) (Bentz and Garboczi, 1990; Garboczi and Bentz, 1992; Bentz, 1997, 2005). CEMHYD3D mimics transport by using a lattice-based algorithm, which allows for solid domains to diffuse through the available pore space and leading to more realistic microstructures. For early age simulations, these aspects have been further improved in the HydratiCA model by Bullard (2007a,b), at cost, however of significantly greater computational requirements. CEMHYD3D introduced various features that make it very relevant to applications. In particular, this model describes explicitly the microstructure of cement paste through a digital image based approach. Scanning electron microscope (SEM) images of the cement of interest are used to construct the initial 3D skeleton. Moreover, each chemical phase present in the cement powder is distinct and represented by a number of cubes/voxels that reproduce the characteristics of the SEM image, respecting the actual PSD. The model is based on a cellular automata algorithm that works through an iterative cycle process, where each voxel that constitutes a phase

can dissolve, diffuse and react when in contact with other voxels. A cycle-to-real time scale factor is to be defined and constitutes the single parameter to be calibrated. CEMHYD3D also includes a large database of different cement types with different Bogue compositions and PSD.

One can naturally argue that macroscale modeling is preferable since it can describe upper scale physical properties, such as the drop of relative humidity in time due to cement hydration. However, subscale features of hydration are only taken into account implicitly in the functional forms. More importantly, all these macroscopic models introduce material parameters that need to be calibrated. Such a calibration process is often tedious and requires up-to-date experimental data for each group of parameters involved in the different mechanisms. Microstructural models are exempt from these constraints even though the major problem lies in the fact that macroscale properties cannot be described or sometimes even defined at that scale.

This study proposes a novel multiscale approach that keeps the advantages of both modeling perspectives. Indeed, in this study, the material parameters in the macroscale formulation are identified from the CEMHYD3D model: the relevant information is extracted and passed from the lower scale to the upper one. This multiscale approach, entitled ONIX model because it requires ONly (the) mIX design as input, has the great advantage of avoiding any parameter calibration. In particular, as demonstrated in this manuscript, it allows the full prediction of self-desiccation in concrete and other cementitious composites. It may also be a useful, straightforward to use, tool for industrial or academic researchers to predict concrete performance.

The proposed approach was presented in a recent conference (Pathirage et al., 2017) and it is here largely extended and commented.

2. Overview of the macro and microscale models

2.1. Macroscale formulation of self-desiccation

The HTC model has been used multiple times in the literature to simulate hydration, heat diffusion and water transport (Di Luzio and Cusatis, 2009a,b), but also for other applications such as aging, self-healing and alkali-silica reaction in concrete (Di Luzio and Cusatis, 2013; Wan et al., 2016; Alnaggar et al., 2017; Di Luzio et al., 2018; Pathirage et al., 2019). In this model, transport phenomena in concrete are modeled at the macroscale through two main governing equations describing heat diffusion and water transport, respectively. The temperature T and relative humidity h fields are computed through the two coupled equations. This manuscript will focus solely on self-desiccation of environmentally sealed samples, thus moisture ingress and concrete drying, both governed by permeability, will have no effect. Consequently, this study does not consider any moisture gradient in space due to an underlying assumption of microstructural homogeneity throughout the samples at length-scales above the hundred of micrometres. Structural details and evolution at smaller length scales will be considered instead using CEMHYD3D.

In the following paragraphs of this section, the original HTC model in the case of sealed concrete will be presented and will be modified compared to its original version to facilitate its subsequent coupling with the CEMHYD3D microscale evolution simulation, and to ensure that the parameter identification problem is well-posed. One can isolate a unit volume of a cementitious composite (concrete, mortar, etc.) and consider the water content w of the isolated volume, which is a function of relative humidity, cement hydration α_c and silica fume reaction degrees α_s. The water content is given by the sum of the evaporable water w_e and the chemically bound water w_n. w_e includes all the phases of evaporable water that exist in concrete, i.e. capillary water, water vapor, adsorbed and hindered adsorbed water. Although transport mechanisms are different for each water phase, a single average transport process is assumed for the sake of simplicity (Di Luzio and Cusatis, 2009a). This process

can be described through a single moisture mass balance equation, which under isothermal and sealed conditions reads

$$\frac{\partial w}{\partial t}(h, \alpha_c, \alpha_s) = 0 \tag{1}$$

or

$$\frac{\partial w_e}{\partial h}\frac{\partial h}{\partial t} + \frac{\partial w_e}{\partial \alpha_c}\dot{\alpha}_c + \frac{\partial w_e}{\partial \alpha_s}\dot{\alpha}_s + \dot{w}_n = 0 \tag{2}$$

In order to simulate self-desiccation in sealed conditions, one needs to impose Neumann no flow boundary conditions, along with prescribing the initial relative humidity $h = 1$ at time $t = 0$ (corresponding to initial saturation at the fresh state). For the sake of simplicity and for the small volume of materials typically considered in self-desiccation tests, the heat diffusion process can be considered fast enough for the entire process to be isothermal (T is constant).

The cement hydration degree, α_c, is defined as the ratio between the mass of cement that has reacted and its initial mass. Such a definition represents an average of the different hydration degrees associated to each individual clinker phase. The expression of its rate is based on the work of Cervera et al. (1999), and can be written as follows

$$\dot{\alpha}_c = A_{c1}\big(A_{c2} + \alpha_c\big)\big\langle \alpha_c^{\infty} - \alpha_c \big\rangle e^{-\frac{\eta_c \alpha_c}{\alpha_c^{\infty}}} e^{-\frac{E_{ac}}{RT}} \tag{3}$$

where A_{c1}, A_{c2} and η_c are material parameters, E_{ac} is the global hydration activation energy and R is the universal gas constant. It is obvious that hydration degree cannot decrease in time. In order to ensure this requirement, the Macaulay brackets $\big\langle x \big\rangle = \max(0, x)$ are used, so that one always has $\forall t \geqslant 0$, $\dot{\alpha}_c(t) \geqslant 0$. Although constant in this study, the temperature and its effect are included in the equation through an Arrhenius law. The internal relative humidity plays an important role in hydration kinetics (Powers and Brownyard, 1946; Bažant and Prasannan, 1989; Bentz, 1997). Unlike the original HTC formulation that considers the

effect of relative humidity through a multiplicative factor in Equation 3, in this study, such an effect is included through the value of the asymptotic degree of hydration.

The expression of the asymptotic degree of hydration α_c^∞ is assumed to decay exponentially for decreasing values of h:

$$\alpha_c^\infty(h) = \tilde{\alpha}_c^\infty e^{-\zeta_c\left(\frac{1}{h}-1\right)} \tag{4}$$

where ζ_c is a material parameter and $\tilde{\alpha}_c^\infty$ is the asymptotic hydration degree in saturated condition ($h = 1$). Finally, Equation 3 must be solved by setting $\alpha_c = 0$ at $t = 0$.

Silica fume is commonly used as a supplementary cementitious material, to generate pozzolanic reactions. These reactions only involve silicon dioxide $SiO_2 = S$, in silica fume and calcium hydroxide, which is one of the cement hydration products. The pozzolanic reactions produce a form calcium-silicate-hydrate, called pozzolanic C-S-H (Mitchell et al., 1998; Bentz, 2000) whose stoichiometry and specific gravity are different to those of conventional C-S-H produced by cement hydration (Cheng-Yi and Feldman, 1985). Similarly to cement hydration degree in Equation 3, one can define the silica fume reaction degree α_s as the mass of reacted silica fume particles over its initial mass. Its evolution in time can be written in a rate form as follows

$$\dot{\alpha}_s = A_{s1}\big(A_{s2} + \alpha_s\big)\big\langle \alpha_s^\infty - \alpha_s \big\rangle e^{-\frac{\eta_s \alpha_s}{\alpha_s^\infty}} e^{-\frac{E_{as}}{RT}} \tag{5}$$

where A_{s1}, A_{s2}, η_s are material parameters and E_{as} is the silica fume reaction activation energy. Equation 5 is solved with the initial condition $\alpha_s(0) = 0$.

Once again, the effect of relative humidity is taken into account through the asymptotic silica fume reaction degree α_s^∞ as

$$\alpha_s^\infty(h) = \tilde{\alpha}_s^\infty e^{-\zeta_s\left(\frac{1}{h}-1\right)} \tag{6}$$

where ζ_s is a material parameter and $\tilde{\alpha}_s^\infty$ is the asymptotic silica fume reaction degree in saturated conditions. One can further define the so-called total reaction degree, α, by combining hydration and silica fume reaction degrees into a single variable, as a measure of the overall C-S-H gel produced. One can write

$$\alpha = \frac{\alpha_c c\tilde{Q}_c^\infty + \alpha_s s\tilde{Q}_s^\infty}{c\tilde{Q}_c^\infty\tilde{\alpha}_c^\infty + s\tilde{Q}_s^\infty\tilde{\alpha}_s^\infty} \tag{7}$$

where c and s are respectively the cement and silica fume contents. $\tilde{Q}_c^\infty$ is the latent heat of hydration reaction per unit of hydrated cement mass. Therefore, the rate of heat generation per unit volume due to cement hydration, $\dot{Q}_c$, is given by $\dot{Q}_c = \dot{\alpha_c} c\tilde{Q}_c^\infty$ (Cervera et al., 1999). It is commonly assumed (Ulm and Coussy, 1995; De Schutter and Taerwe, 1995; Cervera et al., 1999; Gawin et al., 2006a) and experimentally observed (Bentz and Stutzman, 1994) that $\tilde{Q}_c^\infty$ is constant for a given concrete. Its value depends on the initial phase composition of the cement, and can be computed as $\tilde{Q}_c^\infty = \sum_{k=1}^n Q_k^\infty w_k$ where n is the number of compounds in the cement, Q_k^∞ is the individual enthalpy of reaction for each compound and w_k is the associated initial weight percentage (Di Luzio and Cusatis, 2009a). Similarly, $\tilde{Q}_s^\infty$ represents the enthalpy of silica fume reaction per unit of reacted mass and is assumed constant. The rate of heat generation per unit volume due to silica fume reaction, $\dot{Q}_s$, is defined as $\dot{Q}_s = \dot{\alpha_s} s\tilde{Q}_s^\infty$ (De Schutter and Taerwe, 1995).

It is well-known that hydration degree and chemically bound water w_n can be assumed to be proportional. Indeed, a way to measure experimentally hydration degree is through a loss on ignition (LOI) test. By heating concrete above 105°C, all the evaporable water is lost and as a consequence, only the non-evaporable water remains. A temperature as high as 1000°C is needed for the non-evaporable to be completely removed from the concrete solid skeleton: this temperature is called ignition. Thus, the measurement of the weight loss difference at 105°C and at ignition corresponds to the chemically bound water content

(Fagerlund, 2009). Knowing w_n experimentally, one can then deduce experimentally the hydration degree through the following equation

$$w_n = \kappa_c \alpha_c c \tag{8}$$

where κ_c is the mass ratio of non-evaporable water at full hydration and c is the cement content. Equation 8 does not include the negligible effect of silicate polymerization, i.e. the length increase of the C-S-H silicate chains which causes a long term reduction of chemically bound water (Zhang and Gjørv, 1991; Brough et al., 1996). Aside from polymerization, one can find discordant points of view in the literature concerning the direct effect of pozzolanic reaction on the amount of non-evaporable water in the C-S-H. Sellevoid (1987) states that this amount produced by such reaction is similar to the one contained in the CH. On the other hand, Diamond (1983) suggests from experimental evidences that the non-evaporable water content increases in cement pastes that contain silica fume, whereas Li et al. (1996) found a reduction in chemically bound water when silica fume is added to concrete. For the sake of simplicity, it is here assumed as in Powers and Brownyard (1946), that the amount of reacted silica does not affect the non-evaporable water content.

To complete the description of Equation 1, one needs to provide a relationship between evaporable water w_e and relative humidity h.

This relationship is quantified by the adsorption/desorption isotherms. In environmentally sealed conditions, one expects relative humidities above 0.7-0.8, otherwise hydration ceases (Flatt et al., 2011). Hence hysteresis, i.e. the difference between adsorption and desorption would be limited due to the small range of humidities covered. It is thus assumed, as a first approximation, and similarly to Xi et al. (1994), that adsorption and desorption isotherms are similar enough to model both processes through a single so-called sorption isotherm. Masoero et al. (2018) recently raised other concerns on the nanoscale

morphology of the C-S-H gel that influences self-desiccation and sorption isotherms. One solution suggested by the authors, however out of the scope in this work, is to extend the microstructural development models by considering information on the nanostructure evolution. Several models of sorption isotherms were proposed (Brunauer et al., 1938; Mainguy et al., 1999; Baroghel-Bouny et al., 1999; Pinson et al., 2015; Masoero et al., 2018) in order to consider the combination of factors that influence the shape of the isotherms. The formulation implemented in the current macroscale model is based on the phenomenological expression of Nilsson and Mjörnell (2005), which explicitly takes into account the evolution of hydration on the one hand, and silica fume reaction on the other, and separates the contribution of the evaporable water in the C-S-H gel w_e^{gel} and the capillary water w_e^{cap} through

$$w_e = w_e^{gel} + w_e^{cap} \tag{9}$$

The evaporable water in the C-S-H gel, determined by the so-called gel isotherm reads as

$$w_e^{gel} = g_2 \alpha \left(c\tilde{\alpha}_c^{\infty} + s\tilde{\alpha}_s^{\infty} \frac{\tilde{Q}_s^{\infty}}{\tilde{Q}_c^{\infty}} \right) \left[1 - e^{-10\tilde{\alpha}_c^{\infty}(g_1 - \alpha)h} \right] \tag{10}$$

whereas the capillary water, or capillary isotherm, reads

$$w_e^{cap} = \frac{w_0 + \Delta w - w_n - \tilde{w}_e^{gel}}{\left[e^{10\tilde{\alpha}_c^{\infty}(g_1 - \alpha)} - 1 \right]} \left[e^{10\tilde{\alpha}_c^{\infty}(g_1 - \alpha)h} - 1 \right] \tag{11}$$

where g_1 and g_2 are two additional material parameters, w_0 is the initial water content (defined as $w_0 = (w/c)c$), $\tilde{w}_e^{gel}$ denotes the gel isotherm at saturation, i.e. $\tilde{w}_e^{gel} = w_e^{gel}(h = 1)$. The capillary isotherm is derived from a mass balance equation, described later in Section 3 and this explains the presence of the term Δw that defines the mass of water to be supplied to compensate chemical shrinkage and maintain saturated conditions. The functional form

of Δw is

$$\Delta w = \kappa_{sh}\left[\left(1 - \frac{\tilde{Q}_c^{\infty}}{\tilde{Q}_s^{\infty}}\right) c\alpha_c + s\alpha_s\right] \tag{12}$$

where κ_{sh} is a material parameter.

The combination of Equations 1, 3, 5, 7, 8 and 9 allows the calculation of the relative humidity evolution in time. The numerical integration of the governing equation (Equation 1) is carried out by using a finite element approach as described by Di Luzio and Cusatis (2009b).

2.2. The microscale CEMHYD3D model

In order to identify the material parameters of the macroscale model, one needs now to investigate microscale phenomena. CEMHYD3D generates a digitized microstructure of size 100×100×100 µm^3, made out of a cubic grid of 1 µm^3 size units called voxels, and obtained from the water to cement ratio, PSD and phase fractions of the different clinker phases and other hydration reactants. Individual cement particles are represented by a collection of voxels and are randomly placed inside the simulation box, until the target water to cement ratio and PSD are obtained. Periodic boundary conditions are imposed to avoid any boundary-related spurious effect (see Bentz and Stutzman (1994) for details regarding the algorithm).

Once the initial suspension of cement particles is created, the algorithm uses images from SEM to assign each voxel with a specific type of reactant (Bentz and Stutzman, 1994), namely C_3S, C_2S, C_3A, C_4AF, C-$\overline{S}$-H_2 (in three forms: anhydrite C$\overline{S}$, dihydrate C-$\overline{S}$-H_2 and hemihydrate C-$\overline{S}$-$H_{0.5}$), S and H (see notation in Table 1).

The model is now ready to "hydrate" the digitized cement paste. Hydration is simulated as a sequence of configurational changes called cycles. Each cycle involves three steps: dissolution, diffusion, and precipitation. The conversion from cycle number to time is performed through a single parameter β at the end of a simulation. The relationship is a parabolic

Table 1: Designation and properties of cement coumpounds involved in hydration.

Compound Designation	Notation	Density	Heat of hydration	Coefficient to compute non-evaporable water content
		[g/cm^3]	[kJ/kg]	[g water/g cement phase]
Tricalcium silicate	C_3S	3.21 (a)	517 (a,e)	0.24 (c)
Dicalcium silicate	C_2S	3.28 (a)	262 (a,e)	0.21 (c)
Tricalcium aluminate	C_3A	3.03 (a)	1144 (a,e)	0.40 (c)
Tetracalcium aluminoferrite	C_4AF	3.73 (a)	725 (a,f)	0.37 (c)
Gypsum	C-$\overline{S}$-H_2	2.32 (a)	132-187* (b)	0.0**
Silicon dioxide	S	2.20 (a)	780 (b)	0.0 (d)
Calcium silicate hydrate	$C_{1.7}SH_4$	2.12 (a)	-	0.0
Pozzolanic calcium silicate hydrate	$C_{1.1}SH_{3.9}$	1.69 (a)	-	0.0
Calcium hydroxide	CH	2.24 (a)	-	0.0
Ettringite	$C_6A\overline{S}_3H_32$	1.70 (a)	-	0.0
Monosulfate	$C_4A\overline{S}H_12$	1.99 (a)	-	0.0
Hydrogarnet	C_3AH_6	2.52 (a)	-	0.0
Iron hydroxide	FH_3	3.00 (a)	-	0.0

*Hemihydrite and anhydrite respectively, **assumed, -not used, (a) Bentz (1997), (b) Bentz (2000), (c) Molina (1992), (d) Powers and Brownyard (1946), (e) Garboczi and Bentz (1992), (f) Scrivener (1986). Cement chemistry notations: CaO = C, SiO_2 = S, Al_2O_3 = A, Fe_2O_3 = F, H_2O = H and SO_3 = $\overline{S}$.

function that is written as $t_{real} = \beta n_{cycle}^2$ where t_{real} is the real time in hours and n_{cycles} is the number of cycles. Despite this fitting of time, the model retains the ability to predict the sequence of configurational changes in the microstructure. Different values for β (in hours/cycles^2) are reported in the literature and were obtained by calibrating the aforementioned nonlinear function against experimental data from either the evolution in time of the hydration degree or the heat release or the non-evaporable water content. The following values are typically reported: 0.00027 (Bentz, 2006b), 0.00030 (Bentz, 2000; Bentz et al., 2000), 0.00036 (Bentz et al., 2000), 0.000437 (Princigallo et al., 2003) and 7 different values ranging from 0.00022 to 0.00043 (Bentz, 2007). In order to make ONIX a parameter-free model, the most commonly used value of the cycle to time factor, i.e. $\beta = 0.00035$ hours/cycles^2 (Bentz, 1997, 2000, 2005, 2006a; Chen et al., 2007), was selected and fixed throughout the current study.

Dissolution is represented as the conversion of a solid voxel (e.g. the above-listed hydration reactants, such as C_3S) into one or more "packets" of diffusing species, each with size of one voxel. Diffusion is not required to satisfy volume balance, which is instead recovered

during the latter stage of precipitation. The chemistry of the packets of diffusing species depends on the dissolved species. For example, C_3A dissolves into C_3A packets, whereas C_3S produces both CH and $C_{1.7}SH_4$ packets. In reality, dissolution leads to individual ions diffusing in solution and generating a continuous concentration field. The dissolution implemented in CEMHYD3D is thus conceptual and simplified: a detailed implementation of ion-by-ion dissolution can be found in HydratiCA (Bullard, 2007a,b), to the detriment of computational efficiency.

All the solid voxels in the simulation box, both hydration reactants and products, are candidates for dissolution. The probability for each of them to dissolve is given by the product of three factors. The first factor is a solubility flag, set to 0 for phases that are treated as insoluble (e.g. C-S-H) and to 1 for soluble phases (e.g. C_3S but also some hydration products such as CH). The second factor is either a constant or a function of the amount of certain dissolved species in solution: this factor mimics the chemical kinetics of different reactions, e.g. C_3S dissolution being faster than C_2S dissolution (this approximates what other simulations treat explicitly, e.g. HydratiCA or, at the smaller nanoscale, the coarse-grained simulations in Shvab et al. (2017)). The third factor is the number of first-neighbour voxels, around the dissolution candidate, that pertain to the pore space. This factor ensures that only voxels that are in contact with the pore space can dissolve, and that the dissolution probability is proportional to the local solid-pore surface area.

Diffusion of species in solution is approximated as a one-step random walk of the one-voxel species within the voxels pertaining to the pore space. Each diffusing voxel is treated independently, since in CEMHYD3D, each voxel can only be occupied by a single solid, diffusing, water or air (empty porosity) species. It is also important to note that diffusion can only occur in the water-filled porosity, and thus does not occur through any voxels containing a solid, including C-S-H. At this stage, only the initial reactants are present in

the microstructure and the possible chemical reactions read as follows

$$C_3S + 5.3H \longrightarrow C_{1.7}SH_4 + 1.3CH \tag{13}$$

$$C_2S + 4.3H \longrightarrow C_{1.7}SH_4 + 0.3CH \tag{14}$$

$$C_3A + 6H \longrightarrow C_3AH_6 \tag{15}$$

$$C_4AF + 10H \longrightarrow C_3AH_6 + CH + FH_3 \tag{16}$$

One can notice that silica dissolution is not considered, but diffusing CH can react at a silica surface (Equation 21). The volume stoichiometry of each reaction is on average respected after simple considerations of number of moles in the reaction and molar volumes of each compound. As an example, one can take the case of the aluminate reaction (Equation 15). If 1 voxel of C_3A is dissolved, 1.69 voxels of C_3AH_6 are thus produced. In reality, the number of voxels produced can be higher or lower and is associated to a probability, which ensures that in average, for a collection of 100 voxels of C_3A, 169 voxels of C_3AH_6 are indeed produced. Once the dissolution occurs, diffusing entities corresponding to the previously listed chemical reactions proceed with a one-step random walk in the pore space available. It is worth mentioning that a diffusing voxel represents a group of ions of size 1 μm^3, as opposed to individual ions.

Precipitation can occur via three mechanisms: (i) homogeneous nucleation, where a diffusing species is directly converted into a hydration product; only some diffusing species can undergo this process, e.g. CH, whereas other cannot, e.g. C-S-H, (ii) heterogeneous precipitation, where the diffusing species can convert to hydration product only when it comes into contact with certain other solid voxels, e.g. $C_{1.7}SH_4$ can precipitate only when it comes into contact with either C_3S, C_2S, or other voxels of already precipitated C-S-H, (iii) collision-based reaction, where the diffusing species can generate hydration products only

upon collision with a voxel of either another specific diffusing species, or another specific solid phase (e.g. diffusing CH colliding with a silica voxel S to form $C_{1.1}SH_{3.9}$). In the latter case, the possible chemical reactions possible for the diffusing species are

$$C_3A + 3C\overline{S}H_2 + 26H \longrightarrow C_6A\overline{S}_3H_{32} \tag{17}$$

$$2C_3A + C_6A\overline{S}_3H_{32} + 4H \longrightarrow 3C_4A\overline{S}H_{12} \tag{18}$$

$$C_4AF + 3C\overline{S}H_2 + 30H \longrightarrow C_6A\overline{S}_3H_{32} + CH + FH_3 \tag{19}$$

$$2C_4AF + C_6A\overline{S}_3H_{32} + 12H \longrightarrow 3C_4A\overline{S}H_{12} + 2CH + 2FH_3 \tag{20}$$

$$1.1CH + S + 2.8H \longrightarrow C_{1.1}SH_{3.9} \tag{21}$$

$$C_{1.7}SH_4 + 0.5H \longrightarrow C_{1.1}SH_{3.9} + 0.6CH \tag{22}$$

As mentioned earlier, Equation 21 represents the pozzolanic reaction between calcium hydroxide and silica to produce pozzolanic $C_{1.1}SH_{3.9}$, whose composition differs from that of conventional $C_{1.7}SH_4$. The latter, upon contact with water, can also transform to pozzolanic C-S-H (Equation 22), liberating additional CH to participate in Equation 21 (Bentz, 2000). Similar to the dissolution stage, a precipitation reaction occurs with a probability that is either constant or a function of the amount of certain diffusing species in solution, to mimic the chemical kinetics of the various reactions. Equations 17 to 22 entail volume changes which may not be respected locally by each individual reaction in the simulation, due to the voxel resolution: for example, if 100 precipitation reactions occur at different locations during a cycle, each of which entails the appearance of 0.7 volume voxels of species A and the disappearance of 0.5 volume voxels of species B, the simulation will generate A-voxels only at 70 locations (out the 100 where the reactions have occurred) and will remove B-voxels only at 50 locations, in such a way that the volume balance is respected on average in the whole

simulation box. Finally, after a fixed user specified, number of diffusion steps (Bentz, 2000), a new cycle starts. A linked list of active diffusing species is maintained throughout the hydration simulation so that they may remain in solution from one dissolution cycle to the next one. It is only during the last cycle of hydration that all diffusing species are converted to hydration products. CEMHYD3D allows for adiabatic, semi-adiabatic and isothermal conditions. In this study, only the isothermal condition is considered. Moreover, hydration can occur in either saturated or sealed conditions. In saturated condition, the pores emptied by chemical shrinkage are filled with water at each cycle until the capillary pores are depercolated in the three spatial directions. It is important to note that depercolation is a global state and no edge or boundary effects are considered. In sealed condition, instead, some of the voxels corresponding to capillary pores are emptied and, to simulate near-equilibrium conditions during self-desiccation, CEMHYD3D redistributes the remaining water to ensure that the first voxels to be emptied are those pertaining to the largest still water-filled pores, then drying up those that pertain to progressively smaller pores.

Ultimately, a CEMHYD3D simulation provides the temporal evolution of the volume fractions of all the reactive phases and hydration products (see Table 1), enabling one to compute degree of hydration, chemical shrinkage, heat release rate, evaporable and chemically bound water contents, and other quantities that will be relevant for the macroscale model.

3. Bridging the two length scales: the ONIX model

3.1. Necessity of a multiscale framework

As explained previously in Section 2, the macroscale model for self-desiccation introduces several material parameters that need calibration. One can classify them into three groups. Groups 1 and 2 comprise the parameters related to the two evolution laws of hydration degree and silica fume reaction degree respectively; group 3 comprises the parameters that

are involved in the various constitutive relations of water phases and heats of reaction.

Table 2: Parameters of the macroscale model to be identified.

	Par.	Units	Identification	Value
Group 1	A_{c1}	[1/h]	Calorimetric/LOI	$\star$
	A_{c2}	[-]	Calorimetric/LOI	0.005
	η_c	[-]	Calorimetric/LOI	$\star$
	$\tilde{\alpha}_c^\infty$	[-]	Calorimetric/LOI	$\star$
	E_{ac}	[kJ/mole]	Calorimetric	40.00
	ζ_c	[-]	Calorimetric/LOI	$\star$
Group 2	A_{s1}	[1/h]	Calorimetric/LOI	$\star$
	A_{s2}	[-]	Calorimetric/LOI	0.05
	η_s	[-]	Calorimetric/LOI	$\star$
	$\tilde{\alpha}_s^\infty$	[-]	Calorimetric/LOI	$\star$
	E_{as}	[kJ/mole]	Calorimetric	83.14
	ζ_s	[-]	Calorimetric/LOI	$\star$
Group 3	κ_c	[-]	LOI	$\star$
	g_1	[-]	Sorption isotherms	1.50
	g_2	[-]	Sorption isotherms	$\star$
	κ_{sh}	[-]	Geiker/Tazawa methods	$\star$
	$\tilde{Q}_c^\infty$	[kJ/kg]	Calorimetric/ Heat of solution	$\star$
	$\tilde{Q}_s^\infty$	[kJ/kg]	Calorimetric/ Heat of solution	780.00

Par: Parameter, LOI: Loss On Ignition, $\star$ identified from the CEMHYD3D model

Table 2 shows that the macroscale model requires the calibration of 18 parameters in total. Calibrating these parameters from experiments requires at least 4 different tests: groups 1 and 2 require either adiabatic calorimetric tests to monitor the rise in temperature or the heat released, or loss on ignition tests (Bentz et al., 1997; Cervera et al., 1999; D'aloia and Chanvillard, 2002; Nilsson and Mjörnell, 2005). Group 3 requires loss on ignition tests to estimate the non-evaporable water content, but also sorption isotherms tests (Nilsson and Mjörnell, 2005). Chemical shrinkage also needs to be measured separately using the methods described by Geiker (1983) or Tazawa et al. (1995). Finally, the reaction enthalpies require either measurements of heat of solution (Newman, 1950) or calorimetric tests (Livesey et al., 1991). Literature data rarely provide this whole set of measurements for a specific cement

paste, and up-to-date data also happen to be scarce.

An effective way to overcome the aforementioned limitation is to determine these parameters from a microscale perspective. First of all, it is possible to fix the values (see Table 2) of hydration activation energy assumed as an equivalent activation energy that comprises the different activation energies of each cement powder phase (Bentz, 1997) and the activation energy of silica fume reaction (Bentz et al., 1998). The enthalpy of silica fume reaction $\tilde{Q}_s^{\infty}$ can be also fixed (Bentz et al., 1998). The values are identical to the ones that CEMHYD3D uses, and are assumed constant for different types of cement. The two functional forms in Equations 3 and 5 are able to describe well hydration and silica fume reaction degrees, as shown later in the study. It was observed however that the first few hours of hydration are not fully captured. In order to keep the formulation simple, the parameters that control the initial part (first 24 hours) of the hydration and silica fume reaction degrees as functions of time, namely A_{c2} and A_{s2}, can also be fixed based on Di Luzio and Cusatis (2009b). Last but not least, the effect of the parameter g_1 involved in the sorption isotherms (Equations 10 and 11) can be assumed fixed since it cannot be obtained from the CEMHYD3D model and because its optimal value is fairly constant from data analysis of different cement composites (Di Luzio and Cusatis, 2009b).

In total, 12 model parameters remain and their identification using the CEMHYD3D model is described next.

3.2. Parameter upscaling workflow

A specific strategy is needed in order to fully take advantage of the inputs and outputs of the CEMHYD3D and the macroscale models. Concerning the inputs, the database provides the designations of the different cements, in the case where only the type of cement is known. Further knowledge on the Blaine fineness is preferable to perform the cement selection more accurately. Alternatively if the cement oxide composition is known, one can estimate the Bogue composition through the following equations

$$C_3S = 4.0710 \times C - 7.6024 \times S - 6.7187 \times A - 1.4297 \times F \tag{23}$$

$$C_2S = 2.8675 \times S - 0.7544 \times C_3S \tag{24}$$

$$C_3A = 2.6504 \times A - 1.6920 \times F \tag{25}$$

$$C_4AF = 3.0432 \times F \tag{26}$$

In the above equations, F corresponds to Fe_2O_3 and A to Al_2O_3. The equations are solved simultaneously, which allows the determination of the four different clinker phases. Since there are several other underlying assumptions, the reader can refer to Taylor (1997) for more details. Once the composition is estimated, one can choose the closest cement type among the 27 available in the CEMHYD3D model database (Bentz, 2005).

The first step consists in running the CEMHYD3D model at saturated condition ($h = 1$). The length of the simulation is fixed to 10,000 cycles, which represents approximately 4 years in real time, in order to capture the long term evolution of the microstructure.

Once the simulation terminates, ONIX extracts the relevant model outputs, and by keeping track of the number of voxels at each cycle and knowing the initial quantities and densities, it computes hydration degree and silica fume reaction degree using the same definitions as in the macroscale model. The evaporable water in the C-S-H gel is computed similarly. In addition, chemical shrinkage and heat of hydration are calculated based on the different molar volumes, heats of formation (listed in Table 1), and the aforementioned chemical reactions. The chemically bound water content is also estimated knowing that it is proportional to the mass of reacted clinker phases through the coefficients given in Table 1. ONIX then proceeds to an automatic parameter identification process. The identifications are here carried out using the non-linear least square method. If one considers an output $\mathbf{y}^j$ of CEMHYD3D as a function of another output $\mathbf{x}^j$, one can first equally discretize them and

define the values y_i^j and x_i^j at index i of the curve j. Furthermore, if one denotes with f^j the corresponding functional form j in the macroscale formulation, and with $\mathbf{p}^j = \{p_1^j, ..., p_n^j\}$ the n^j unknown parameters, one can formulate the minimization problems as follows

$$\text{Find } \mathbf{p}^j \text{ that minimizes } \varphi^j = \sum_{i=0}^{N} \left(y_i^j - f^j(x_i^j, \mathbf{p}^j)\right)^2 \tag{27}$$

where φ^j is the objective function for the curve j and N is the number of discretized points. In order to perform this minimization process, the simplex algorithm (Nelder and Mead, 1965) is used. For example. in the case of hydration, f^3 is defined through Equation 3, $\mathbf{x}^3$ is the hydration degree, $\mathbf{y}^3 = \dot{\mathbf{x}}^3$ is its time rate and $\mathbf{p}^3 = \{A_{c1}, \eta_c, \tilde{\alpha}_c^\infty\}$.

An example shows such a process, that is later used for one self-desiccation prediction (see Figure 2f, $w/c = 0.36$ and $s/c = 0.10$). Figures 1a,b,c,d show the identified curves for each evolution law listed previously, at saturated condition. It is worth pointing out that since the outputs of the CEMHYD3D model are relevant to cement paste, a volume conversion is needed in the cases of mortar and concrete, for which the aggregate to cement ratio is known. A more detailed analysis on the effect of aggregate could be performed, but it is outside the scope of this study. For instance, the presence of water in the aggregate may affect the non-evaporable content and available corrections (Fagerlund, 2009) could be taken into account. Moreover, in the proposed framework, the mechanical interaction between aggregates and cement paste is not considered, and although the aggregate shape and grading affect autogeneous shrinkage (Rasoolinejad et al., 2019), they are not important as far as self-desiccation is concerned.

The latent heat of hydration $\tilde{Q}_c^\infty$ is identified by computing the initial masses of the different clinker phases. The curves of cement hydration and silica fume reaction degrees as functions of time (Figure 1a) allow the identification of all the parameters in groups 1 and 2, with the exception of ζ_c and ζ_s, which requires a separate procedure described later in this

section. The parameters in group 3 are then determined, starting with κ_c that is identified from the non-evaporable water vs hydration degree curve (Figure 1b). w_n is here plotted as a function of total reaction degree, as opposed to cement hydration degree. The gradient of $w_n(\alpha)$ displays a small but meaningful increase at about $\alpha = 0.75$, which corresponds to the plateau of silica fume reaction degree. Indeed, the number of water voxels available for the dissolution of C_3S, C_2S, C_3A and C_4AF increases when all the silica fume voxels are consumed in the pozzolanic reaction, and consequently engenders an increase of the mass of reacted clinker phases. κ_{sh} is identified from the chemical shrinkage vs total reaction degree curve (Figure 1c) and g_2 from the evaporable water in the C-S-H gel vs total reaction degree curve (Figure 1d).

At the end of this phase, only two parameters are yet to be determined: ζ_c and ζ_s. The CEMHYD3D model is again used but in sealed condition for which the capillary pores are not water-filled at each cycle. This allows the identification of the latter two parameters from cement hydration and silica fume reaction degrees vs time curves respectively, which are now different from the curves corresponding to saturated conditions. The fact that the CEMHYD3D model is limited to sealed or saturated conditions does not narrow the applicability of ONIX. Indeed, the relevant parameters related to the relative humidity variation are all identified. The formulations in the HTC model then allow any external environmental conditions applied to the defined finite element domain boundaries. In the case of non-uniform relative humidity, the permeability plays of course a large role and the associated parameters are to be identified from either experimental data or from the published literature.

3.3. Mass conservation verification

One can notice that the evolution of evaporable water in the capillaries (Figure 1e) is not fitted because it is simply a consequence of the identification process previously described: the only parameter involved in Equation 11 is indeed g_2 (because g_1 has been assumed

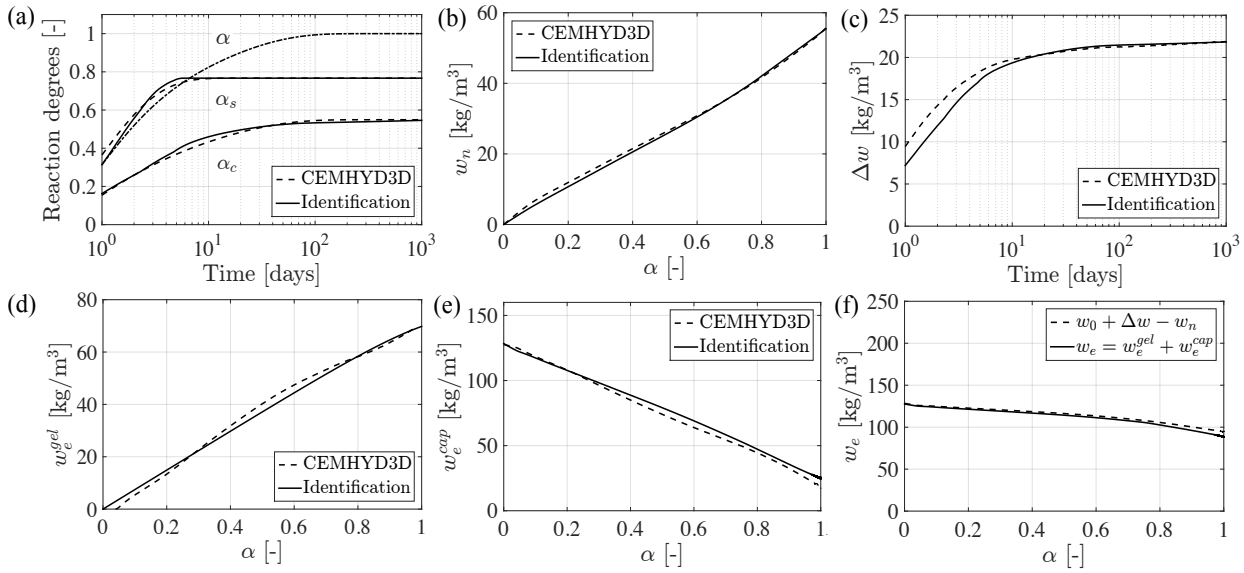

Figure 1: Parameter identification procedure on an example: Persson (1996), Figure 2f, $w/c = 0.36$ and $s/c = 0.10$. (a) cement and silica fume reaction degrees as a function of time, (b) chemically bound water content as a function of total reaction degree, (c) chemical shrinkage as a function of time, (d), (e) and (f) evaporable water in the C-S-H gel, in the capillaries and total evaporable water, respectively, as a function of total reaction degree.

constant, see Section 3) and is identified through the evaporable water in the C-S-H gel. Such a match of w_e^{cap} (Figure 1e) is achieved because Equation 11 translates a mass balance. Indeed, the amount of water needed to ensure saturated condition and the total water content must be equal. This mass conservation principle can be written as

$$w_0 + \Delta w = w_e + w_n \tag{28}$$

where Δw and w_n have been already identified earlier. Figure 1f shows the total evaporable water w_e as a function of the total reaction degree. One can see that Equation 28 is respected at any time, for both the macroscale model and CEMHYD3D. As expected, the non-evaporable water, the chemical shrinkage and the evaporable water in the C-S-H gel increase, while the evaporable water in the capillaries and the total evaporable water decrease in time, as a direct result of hydration.

4. Parameter-free model predictions

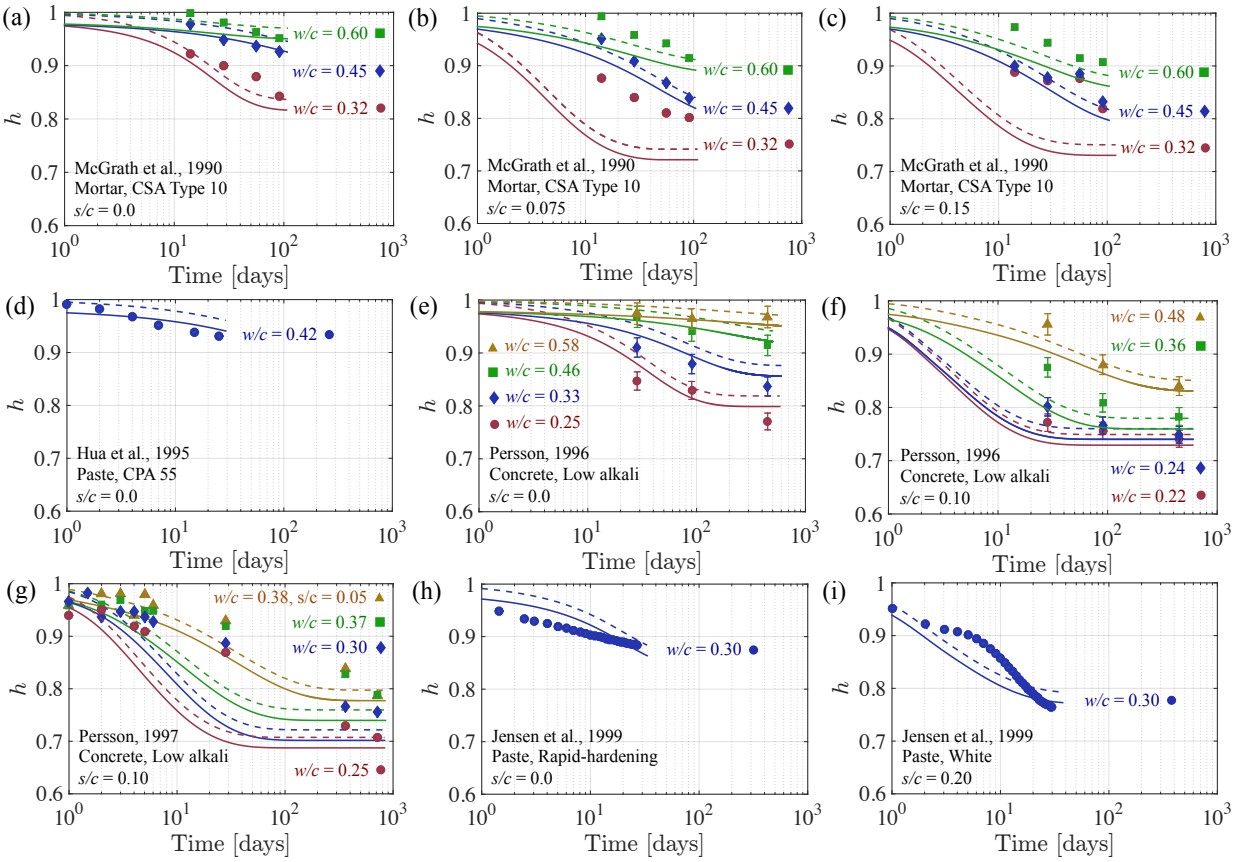

Figure 2: Prediction of self-desiccation. Markers represent experimental data, dashed and solid curves are respectively the predictions using an initial relative humidity value of $h = 1$ (upper bound) and $h = 0.98$ (lower bound). (a), (b) and (c) McGrath and Hooton (1990), (d) Hua et al. (1995), (e) and (f) Persson (1996) where error bar represent respectively +/-5% in humidity (absolute), (g) Persson (1997), (h) and (i) Jensen and Hansen (1999).

In order to validate the proposed ONIX model, a vast collection of experimental data available in the literature is considered. The set of data contains self-desiccation results for 49 different cementitious composites and for all of them, relative humidity was measured on sealed specimens at room temperature. Figures 2, 3 and 4 show the full prediction results. The figures appear in chronological order and are plotted in semi-logarithm scale to highlight the long-term nature of self-desiccation. The first 24 hours are omitted due to the lack of accuracy in the identification procedure prior to that age (see Section 3). For

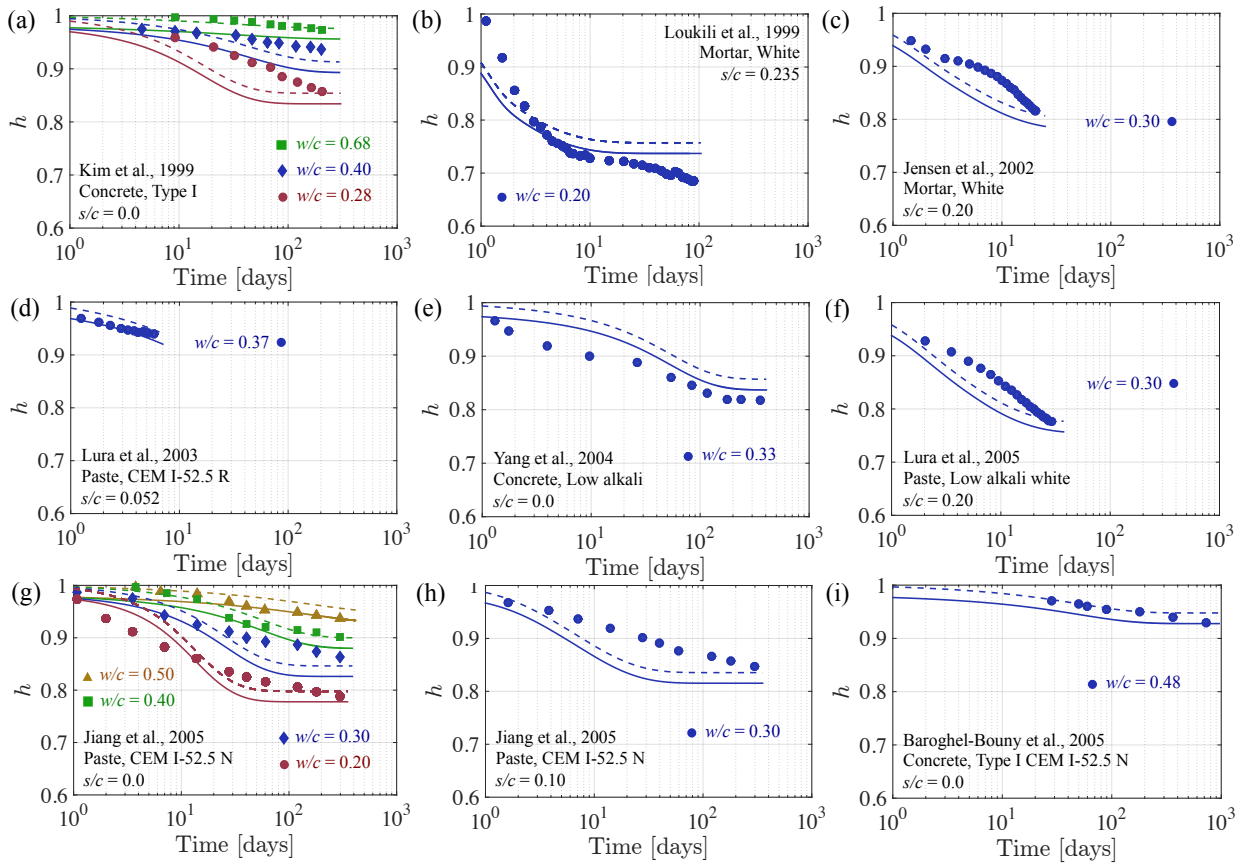

Figure 3: Prediction of self-desiccation. Markers represent experimental data, dashed and solid curves are respectively the predictions using an initial relative humidity value of $h = 1$ (upper bound) and $h = 0.98$ (lower bound). (a) Kim and Lee (1999), (b) Loukili et al. (1999), (c) Jensen and Hansen (2002), (d) Lura et al. (2003), (e) Yang and Zhang (2004), (f) Lura et al. (2005), (g) and (h) Jiang et al. (2005), (i) Baroghel-Bouny and Mounanga (2005).

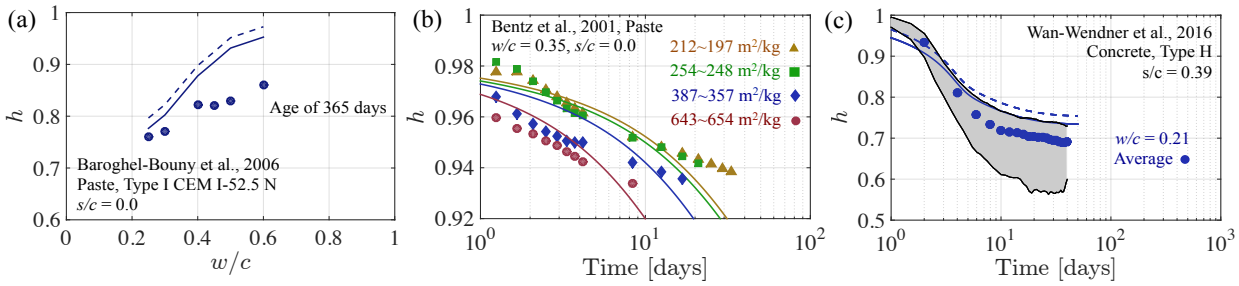

Figure 4: Prediction of self-desiccation. Markers represent experimental data, dashed and solid curves are respectively the predictions using an initial relative humidity value of $h = 1$ (upper bound) and $h = 0.98$ (lower bound). (a) Baroghel-Bouny et al. (2006), (b) Bentz et al. (2001) where four different Blaine finenesses were tested, (actual experimental value $\sim$ simulated value). The initial relative humidity was estimated to be $h = 0.98$ and therefore only the associated prediction is shown in solid curves, (c) Wan et al. (2016) where the gray area represents the upper and lower bounds of the experimental curves, and markers represent the average.

further details on the identified values of the parameters, the reader can refer to the attached supplementary material.

When a concrete sample is still at fresh state and environmentally sealed, there is first an increase of humidity as the sensor placed within the specimen equilibrates with the concrete pore solution. The relative humidity then reaches a plateau, at about $h = 0.98$ before decreasing, due to cement hydration. It is reported in the literature that the initial relative humidity is never $h = 1$ and that the plateau is due to the dissolved ions (Ca^+, Na^+, etc.) in the pore solution (Bentz et al., 2001; Lura et al., 2003). The value of humidity in this initial plateau depends on the water to cement ratio and on the cement composition. It may be estimated using Kelvin's equation combined with Raoult's law (Lura et al., 2003) but in most cases, this initial value of relative humidity is between $h = 1$ and $h = 0.98$, where the latter value is more commonly reported for low water to cement ratios. The dashed and solid curves in Figures 2, 3 and 4 are respectively the predictions using an initial relative humidity value of $h = 1$ (upper bound) and $h = 0.98$ (lower bound). Thus, the actual prediction lies in between these two bounds and one can observe a very good agreement with the experimental data. ONIX does not explicitly take into account the mechanisms happening at a scale lower than the resolution provided by the CEMHYD3D model. Considerations of capillary depression, surface tension of colloidal particles or disjoining pressure (Hua et al., 1995) are thus only averaged. A recent work has also shown that the precipitation of hydration products in confined spaces, together with the effect of charged colloidal particles contribute to bulk volume changes (Abuhaikal et al., 2018). ONIX does not capture such phenomena; self-desiccation is only predicted through the evolution of the different water contents, more specifically through the empirical isotherm that relates saturation degree with relative humidity, regardless of the nanostructure of hydrating cement.

5. Discussions

5.1. Effect of w/c and s/c ratios

The effects of w/c and s/c ratios are well captured by ONIX, namely lower w/c ratio and higher s/c ratio both increase self-desiccation. For instance, Figures 2a,c and Figures 3a,g show a clear trend of increasing self-desiccation when the water to cement ratio decreases. The presence of silica fume emphasizes this reduction, for similar w/c ratios (Figures 2e,f).

Not only the relative humidity diminishes for lower w/c ratios, but also the rates of relative humidity drop in time increase. Similarly, a further increase of the rates is observed when silica fume is added (Figures 2e,f).

For fixed cement types, PSD and Blaine finenesses, the increase in w/c ratios induces an increase in the parameters A_{c1}, $\tilde{\alpha}_c^\infty$ and ζ_c. No particular trend is observed for η_c: in some cases, this value increases (Figures 2e,f,g, Figure 3g) and in others, the trend is not clear (Figure 4a). On the other hand, g_2 decreases, along with κ_c. The parameter κ_{sh} for the chemical shrinkage remains constant. It should be noted that when silica fume is added to the mix, κ_{sh} becomes about three times larger, which illustrates the importance of pozzolanic reaction and the increase in the proportion of fine reactants on chemical shrinkage.

The reason why ONIX is able to simulate this behavior is because for low w/c ratios, the asymptotic hydration degree, along with the chemical shrinkage decrease. Indeed, the water content in the capillaries is not enough to obtain full hydration of the clinker phases. The evaporable water in the C-S-H gel is also reduced as a consequence. Furthermore, adding silica fume increases the surface area of the reactants in the CEMHYD3D microstructure and thus accelerates hydration rate. The size of the capillary pores is also captured by the (changing) shape of the sorption isotherm, as a function of w/c or s/c ratio, which in turn contributes to an increase of self-desiccation. Equations 3, 5, 8, 9 and 12 plugged into the moisture mass balance equation (Equation 1) translate the aforementioned changes of the water contents into a more prominent self-desiccation.

The other physical reason at the nanoscale, not captured by ONIX, is that for lower w/c ratios, the pore structure becomes finer. Kelvin's equation thus helps explain the larger decrease of relative humidity (Bentz et al., 2001). Moreover, the addition of silica fume makes the pore structure to become even finer (Sellevold and Justnes, 1992), and therefore further increases the effect of self-desiccation.

5.2. Effect of cement type

The composition of cement plays an important role in hydration, and consequently in self-desiccation. In order to illustrate the effect of cement type, one can for instance compare the drop of relative humidity given in Figure 2a (McGrath and Hooton, 1990) and Figure 2e (Persson, 1996), without silica fume addition, for $w/c = 0.32$ and 0.33 respectively. The difference in w/c is negligible. McGrath and Hooton (1990) used a CSA Type 10 cement, similar to Type I cements, whereas Persson (1996) adopted a low alkali cement. The Bogue compositions for the four major clinker phases C_3S, C_2S, C_3A and C_4AF are 61.69%, 11.31%, 6.52%, 7.25% and 53.0%, 22.50%, 1.42%, 13.4%, for the CSA Type 10 and low alkali cements, respectively. The experimental measurements show that, at age 90 days, the low alkali cement induces a lesser degree of self-desiccation compared to the CSA Type 10 cement. The percentage difference between the two averages is 4.25%. ONIX is able to capture this difference, with a little higher percentage difference of 9%. Indeed, as explained in Section 2, the dissolution probability of C_3S is larger than the other clinker phases, and one can notice that the quantity of C_3S is smaller in the low alkali cement used in Persson (1996). This results in a higher value of $\tilde{\alpha}_c^\infty$ in the case of low alkali cement, for the same final age of four years. The evolution of the microstructure becomes thus different, and results in a larger reduction of relative humidity for the CSA Type 10 cement. On the contrary, Figure 3c (Jensen and Hansen, 2002) and Figure 3f (Lura et al., 2005) show that for close enough cement types, in this case white and low alkali white cements respectively, the minor difference in composition does not affect noticeably self-desiccation.

5.3. Effect of PSD and Blaine fineness

It was previously mentioned that the surface area is a crucial parameter affecting the hydration reaction rates, in both the actual hydrating cement skeleton and in the CEMHYD3D model. The effect of particle size distribution and Blaine fineness of cement was studied (Bentz et al., 2001) and it was found that for the same cement ground to four different finenesses, the finer the cement, the higher the rate of relative humidity decrease at a constant w/c (Figure 4b). This experimental work is here simulated using four different Blaine finenesses similar to the actual ones. One can observe a good agreement between the predictions and data, particularly in terms of trend. The larger pores corresponding to a lower Blaine fineness induce a lower drop of relative humidity. Similarly to the effect of cement type, the effects of Blaine fineness and PSD on self-desiccation are well captured by the model due to the fact that the CEMHYD3D model microstructure is based on the actual particle size distribution. The asymptotic hydration degree does not change whereas the hydration dregree rate increases, i.e. A_{c1} decreases and η_c increases, as opposed to the effect of w/c ratios previously described. It is worth pointing out that in the proposed framework, no approximation is needed, for instance assuming an effective cement particle size.

5.4. Short and long term behavior

Self-desiccation is observed from early ages to many years. One can see that an overall good agreement is achieved, for the entire time span. The decrease of relative humidity in time is monotonic, and a typical S-shaped curve is expected when plotted in semi-logarithmic scale. Depending on the mix design, the final equilibrium is reached but it appears that for some of the collected data, the self-desiccation process continues while the predictions always reach an equilibrium after a certain time period, as shown for instance in Figures 2g or Figures 3h, and it seems that the plateau is reached a little earlier than the experimental values. As an example, one can observe the case used to illustrate the identification process in

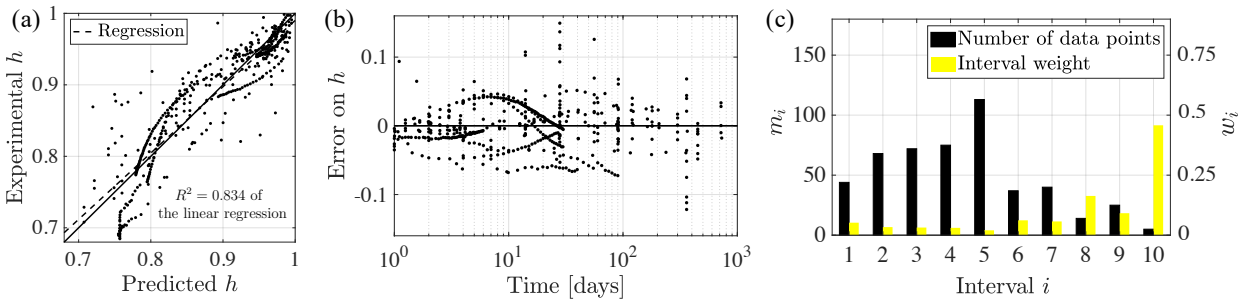

Figure 5: Statistics of the ONIX predictions. (a) Scatter of the measured versus predicted values of h, (b) Error (or residual), i.e. the difference between the measured and the predicted values of h, as a function of time.

Figure 1a and Figure 2f (Persson, 1996) for $w/c = 0.36$ and $s/c = 0.10$. The relative humidity plateaus as soon as the hydration and silica fume reaction degrees reach their asymptotic values, at about 100 days. The reason of the plateau is that the rates of hydration and silica fume reaction degrees become closer to 0. Indeed, the quantity of capillary water decreases as hydration chemical reactions progress in time and becomes insufficient for further reactions.

One explanation is that as hydration occurs, cement hydrates form on and surround anhydrous cement particles, building a shell nearly impermeable that only allows a slow water transport and thus prolongs hydration (Rahimi-Aghdam et al., 2017; Rahimi-Aghdam and Bažant, 2018). The CEMHYD3D model does not consider such a process since diffusion is not allowed through solid particles, as mentioned in Section 2.

It is also worth mentioning that the CEMHYD3D model does not take into account the influence of long term creep and C-S-H modification on internal relative humidity.

Another explanation is that the CEMHYD3D model seems to predict an early plateau of the hydration and silica fume reaction degrees. A change in the cycle-to-time scale factor would certainly help improving the results, however, a calibration process would then be needed. It does not appear necessary to introduce a new level of complexity since the prediction results as such are more than satisfactory.

5.5. Prediction accuracy

All the results shown in this paper are pure predictions, i.e. no parameter fitting using experimental data was performed, and their accuracy varies from set to set, as one can see in Figures 2, 3, and 4. In order to assess the overall accuracy of the predictions, it is convenient to analyze the statistics of the entire database. Figure 5a shows the experimental values of relative humidity plotted against the model predictions for all the results shown in Figures 2,3 and 4. The solid and dashed curves are the identity line and the linear regression, respectively. The linear regression is characterized by a coefficient of determination $R^2 = 0.834$, which indicates that the predicted values are generally well correlated with the measured data. However, R^2 is not a rigorous measure of the prediction accuracy, which instead requires the statistical regression analysis with reference to the identity line (Legates and McCabe Jr, 1999; Bažant and Baweja, 2000).

This task can be handled efficiently by the algorithm devised by Bažant and coworkers with reference to creep and shrinkage data (Bažant and Baweja, 1995, 2000; Bažant and Li, 2008; Bažant and Jirásek, 2018; Rasoolinejad et al., 2019). This approach, based on the method of weighted least square, handles correctly the spurious effect of non-uniform data distribution always plaguing time dependent data sets of concrete response. It is worth observing that the applicability of statistical regression analysis based on least square requires nearly homoscedastic experimental data (Bulmer, 1979; Ang and Tang, 1975). For the self dessication data analyzed in this paper, nearly homoscedasticity can be obtained by using a log time scale.

Figure 5b shows the error (or residual), computed as the difference between the experimental and the predicted values of relative humidity, $e = h^{exp} - h^{pre}$, as a function of time. One can see that for the majority of the data points are below 0.1 in absolute value. The error distribution is clearly non uniform and there are more data points at early ages. This is correlated with having more data points for h close to 1 as visible in Figure 5a.

A remedy to this issue is to define time intervals that are equally spaced in log scale, $\Delta t_i = t_{i+1} - t_i = 2t_i - t_i = t_i$ for $i = 1, ..., 10$; $t_1 = 1$ day, and to compute a weight for each interval as $w_i = 1/(m_i \bar{w})$ (see Figure 5c) where $\bar{w} = \sum_{i=1}^{n} 1/m_i = 0.4370$. The average weighted error is $\bar{e} = (\bar{w}/n) \sum_{i=1}^{n} w_i \sum_{j=1}^{m_i} |e_{ij}| = 0.0221$, which is very small considering that the relative humidity can take values between 0 and 1. Furthermore, following Rasoolinejad et al. (2019), the overall weighted standard deviation of the prediction data and the overall weighted standard deviation of the experimental data read

$$s = \sqrt{\frac{N}{(N-p)} \frac{\bar{w}}{n} \sum_{i=1}^{n} w_i \sum_{j=1}^{m_i} e_{ij}^2} = 0.0338 \tag{29}$$

and

$$\bar{s} = \sqrt{\frac{N}{(N-p)} \frac{\bar{w}}{n} \sum_{i=1}^{n} w_i \sum_{j=1}^{m_i} \left(h_{ij}^{exp} - \bar{h}\right)^2} = 0.0857 \tag{30}$$

respectively, where $N = 494$ is the total number of data points, $p = 0$ is the number of parameters that were identified with the experimental data, and $\bar{h} = (\bar{w}/n) \sum_{i=1}^{n} w_i \sum_{j=1}^{m_i} h_{ij} = 0.875$ is the weighted mean of all the experimental data. Finally, by using s and $\bar{s}$, one can compute the unbiased coefficient of variation of the prediction data, $\omega = s/\bar{h} = 3.87\%$, and the coefficient of determination, $r^2 = 1 - s^2/\bar{s}^2 = 0.844$, with respect to identity line of the h^{exp} versus h^{pre} plot.

These results demonstrate that the numerical predictions are in excellent statistical agreement with the experimental data over the entire database and that the model formulation can intrinsically account for a very large percentage of the data variation.

The prediction error might be due to several reasons that are described briefly below. First of all, the model cannot capture phenomena at nanoscale which is much smaller than the resolution of CEMHYD3D. Moreover, there is no consideration of ITZ between the paste and aggregate particles in the cases of mortar and concrete, that can play a role in the quantity of the different waters consumed and generated (Bentz et al., 1999). As mentioned

earlier, the effect of water contained in the aggregates was also not taken into account.

In addition, some of the experimental data collected, for instance in Figure 3b (Loukili et al., 1999), show peculiar trends. One can observe a typical drop of relative humidity that plateaus at about 30 days followed by an unexpected second drop. The latter drop would either indicate that hydration and/or silica fume reactions are accelerated at this time period, which is unphysical, or that it is simply caused by drying due to a defective sealing of the specimens. For higher w/c and lower s/c ratios, a larger volume of capillary water is present in the paste and if the specimen sealing becomes imperfect after a certain period of time, drying may occur but remains minimal and will not result in a significant drop in humidity. The opposite phenomenon is expected for lower w/c and higher s/c (Figure 3b). Indeed, keeping a concrete sample perfectly sealed throughout the years is challenging and such results may be considered with great attention in order to avoid erroneous conclusions.

Finally, the experiments always display a significant scatter, which is sometimes non-negligible, and limits the accuracy that can be expected from predictions. One of the main reasons of this observed scatter is due in general to the small accuracy of the devices adopted to measure the relative humidity. This scatter is especially noticeable for concrete containing low w/c and high s/c ratios. Figure 4c shows a percentage difference of about 30% at 40 days between the upper and lower curves relevant to two samples having the same mix design. Although this large difference is due to the uncommon mix ratios used for this specific high performance concrete, this observation raises the fact that the scatter in the experiments must be taken into consideration while evaluating the capabilities of a model.

5.6. Computational cost

In general, microstructural development models needs more computational resources than macroscale models, depending on the termination time prescribed for hydration. In order to accurately capture the asymptotic values of hydration and silica fume reaction degrees, ONIX is executed for a long time scale, typically 4 years in real time (see Section 3).

Nevertheless, the model requires only up to 4 hours if launched on a normal desktop computer to complete full hydration and identify the macroscale model parameters. Moreover, once the parameters are identified, there is indeed no need to rerun ONIX calibration during the numerical analysis. As a matter of fact, the time needed for the execution of ONIX is always much smaller than the time required for the parameter identification based on experimental data that requires many experiments to be carried out.

6. Summary and Conclusions

This paper presents the formulation and validation of a novel multiscale approach, entitled the ONIX model, to simulate self-desiccation of concrete, mortar and cement paste. The ONIX model formulates self-dessication by means of a macro-scale mass balance equation involving evaporable water and chemically bound water whose evolution depends on the extent of the cement hydration and the silica-fume reactions. All the parameters governing the aforementioned equation are identified by using the output of micro-scale simulations carried out by the CEMHYD3D model. The ONIX model was validated by predicting self-dessication data of 49 different mix designs, relevant to numerous water to cement ratios, silica fume to cement ratios, cement types, Blaine finenesses and cement particle size distributions. Based on the on the obtained results the following conclusions can be drawn.

- Contrarily to all other models for self dessication available in the literature, the ONIX model does not require any preliminary calibration with experimental data and it uses as input only the mix design of the concrete, mortar, or cement paste to be simulated.

- The predicted variation of relative humidity as function of time is overall in excellent agreement with the experimental data. Indeed, an unbiased statistical comparison of the prediction data versus the experimental data provides a coefficient of variation of the predictions equal to 3.87% and a coefficient of determination of 0.844.

- The ONIX model predicts well, both qualitatively and quantitatively, the effect of the most important mix design parameters controlling self desiccation, namely water to cement ratio, silica fume to cement ratio, cement type, and Blaine fineness.
- Since the ONIX model uses the micro-scale CEMHYD3D model only to identify the parameters of the macro-scale equations, the numerical simulations of self-dessication are computationally inexpensive even for practical, large scale applications.

7. Declarations of interest

The Authors declare that there is no conflict of interest.

8. Acknowledgment

The work of the first and last authors was sponsored by the U.S. Army Engineer Research and Development Center (ERDC) under Contract Number W912HZ-17-C-0027. Permission to publish was granted by the director of the ERDC Geotechnical and Structures Laboratory.

9. References

Abuhaikal, M., Ioannidou, K., Petersen, T., Pellenq, R. J.-M., Ulm, F.-J., 2018. Le châteliers conjecture: Measurement of colloidal eigenstresses in chemically reactive materials. Journal of the Mechanics and Physics of Solids 112, 334–344.

Alnaggar, M., Di Luzio, G., Cusatis, G., 2017. Modeling time-dependent behavior of concrete affected by alkali silica reaction in variable environmental conditions. Materials 10 (5), 471.

Ang, A. H.-S., Tang, W. H., 1975. Probability concepts in engineering planning and design. Vol. 1, Basic principles. No. BOOK.

Baroghel-Bouny, V., Mainguy, M., Lassabatere, T., Coussy, O., 1999. Characterization and identification of equilibrium and transfer moisture properties for ordinary and high-performance cementitious materials. Cement and concrete research 29 (8), 1225–1238.

Baroghel-Bouny, V., Mounanga, P., 2005. Effects of self-desiccation on autogenous deformations, microstructure and long-term hygral behaviour. In: The fourth international research seminar on self-desiccation and its importance in concrete technology, Gaitherburg, Maryland. Vol. 20. pp. 21–48.

Baroghel-Bouny, V., Mounanga, P., Khelidj, A., Loukili, A., Rafai, N., 2006. Autogenous deformations of cement pastes: part ii. w/c effects, micro–macro correlations, and threshold values. Cement and Concrete Research 36 (1), 123–136.

Bažant, Z. P., Baweja, S., 1995. Justification and refinements of model b3 for concrete creep and shrinkage 1. statistics and sensitivity. Materials and structures 28 (7), 415–430.

Bažant, Z. P., Baweja, S., 2000. Creep and shrinkage prediction model for analysis and design of concrete structures: Model b3. ACI Special Publications 194, 1–84.

Bažant, Z. P., Jirásek, M., 2018. Creep and hygrothermal effects in concrete structures. Vol. 225. Springer.

Bažant, Z. P., Li, G.-H., 2008. Unbiased statistical comparison of creep and shrinkage prediction models. ACI materials Journal 105 (6), 610–621.

Bažant, Z. P., Prasannan, S., 1989. Solidification theory for concrete creep. i: Formulation. Journal of engineering mechanics 115 (8), 1691–1703.

Bentz, D., 2005. Cemhyd3d: A three-dimensional cement hydration and microstructure development modeling package. version 3.0.

Bentz, D., 2006a. Modeling the influence of limestone filler on cement hydration using cemhyd3d. Cement and Concrete Composites 28 (2), 124–129.

Bentz, D. P., 1997. Three-dimensional computer simulation of portland cement hydration and microstructure development. Journal of the American Ceramic Society 80 (1), 3–21.

Bentz, D. P., 2000. CEMHYD3D: A three-dimensional cement hydration and microstructure development modelling package. Version 2.0. US Department of Commerce, National Institute of Standards and Technology.

Bentz, D. P., 2006b. Capillary porosity depercolation/repercolation in hydrating cement pastes via low-temperature calorimetry measurements and cemhyd3d modeling. Journal of the American Ceramic Society 89 (8), 2606–2611.

Bentz, D. P., 2006c. Influence of water-to-cement ratio on hydration kinetics: simple models based on spatial considerations. Cement and Concrete Research 36 (2), 238–244.

Bentz, D. P., 2007. Verification, validation, and variability of virtual standards. In: Proceedings of the 12th International Congress on the Chemistry of Cement.

Bentz, D. P., Feng, X., Stutzman, P. E., 2000. Analysis of CCRL proficiency cements 135 and 136 using CEMHYD3D. National Institute of Standards and Technology, Technology Administration .

Bentz, D. P., Garboczi, E. J., 1990. Digitised simulation model for microstructural development. Ceram. Trans. 16, 211–226.

Bentz, D. P., Garboczi, E. J., Haecker, C. J., Jensen, O. M., 1999. Effects of cement particle size distribution on performance properties of portland cement-based materials. Cement and concrete research 29 (10), 1663–1671.

Bentz, D. P., Jensen, O. M., Hansen, K. K., Olesen, J. F., Stang, H., Haecker, C.-J., 2001. Influence of cement particle-size distribution on early age autogenous strains and stresses in cement-based materials. Journal of the American Ceramic Society 84 (1), 129–135.

Bentz, D. P., Snyder, K. A., Stutzman, P. E., 1997. Microstructural modelling of self-desiccation during hydration. Report TVBM-3075 Self-Desiccation and Its Importance in Concrete Technology, Lund University, Lund, Sweden, 132–140.

Bentz, D. P., Stutzman, P. E., 1994. Sem analysis and computer modelling of hydration of portland cement particles. In: Petrography of cementitious materials. ASTM International.

Bentz, D. P., Waller, V., de Larrard, F., 1998. Prediction of adiabatic temperature rise in conventional and high-performance concretes using a 3-d microstructural model. Cement and Concrete research 28 (2), 285–297.

Bishnoi, S., Scrivener, K. L., 2009. μic: A new platform for modelling the hydration of cements. Cement and Concrete Research 39 (4), 266–274.

Bocciarelli, M., Ranzi, G., 2018a. Identification of the hygro-thermo-chemical-mechanical model parameters of concrete through inverse analysis. Construction and Building Materials 162, 202 – 214.

Bocciarelli, M., Ranzi, G., 2018b. An inverse analysis approach for the identification of the hygro-thermo-chemical model parameters of concrete. International Journal of Mechanical Sciences 138, 368–382.

Boumakis, I., Marcon, M., Wan, L., Wendner, R., 2015. Creep and shrinkage in fastening systems. In: CONCREEP 10. pp. 657–666.

Brough, A., Dobson, C., Richardson, I., Groves, G., 1996. Alkali activation of reactive silicas in cements: in situ29si mas nmr studies of the kinetics of silicate polymerization. Journal of materials science 31 (13), 3365–3373.

Brunauer, S., Emmett, P. H., Teller, E., 1938. Adsorption of gases in multimolecular layers. Journal of the American chemical society 60 (2), 309–319.

Bullard, J. W., 2007a. Approximate rate constants for nonideal diffusion and their application in a stochastic model. The Journal of Physical Chemistry A 111 (11), 2084–2092.

Bullard, J. W., 2007b. A three-dimensional microstructural model of reactions and transport in aqueous mineral systems. Modelling and Simulation in Materials Science and Engineering 15 (7), 711.

Bulmer, M. G., 1979. Principles of statistics. Courier Corporation.

Cervera, M., Oliver, J., Prato, T., 1999. Thermo-chemo-mechanical model for concrete. i: Hydration and aging. Journal of engineering mechanics 125 (9), 1018–1027.

Chen, H., Wyrzykowski, M., Scrivener, K., Lura, P., 2013. Prediction of self-desiccation in low water-to-cement ratio pastes based on pore structure evolution. Cement and Concrete Research 49, 38 – 47.

Chen, W., Brouwers, H. J. H., Shui, Z. H., Dec 2007. Three-dimensional computer modeling of slag cement hydration. Journal of Materials Science 42 (23), 9595–9610.
URL https://doi.org/10.1007/s10853-007-1977-z

Cheng-Yi, H., Feldman, R. F., 1985. Hydration reactions in portland cement-silica fume blends. Cement and Concrete Research 15 (4), 585–592.

D'aloia, L., Chanvillard, G., 2002. Determining the apparent activation energy of concrete: Eanumerical simulations of the heat of hydration of cement. Cement and Concrete Research 32 (8), 1277–1289.

de Freitas, J. T., Cuong, P., Rui, F., 2015. Modeling of cement hydration in high performance concrete structures with hybrid finite elements. International Journal for Numerical Methods in Engineering 103 (5), 364–390.

De Schutter, G., Taerwe, L., 1995. General hydration model for portland cement and blast furnace slag cement. Cement and Concrete Research 25 (3), 593–604.

De Schutter, G., Taerwe, L., 1996. Degree of hydration-based description of mechanical properties of early age concrete. Materials and Structures 29 (6), 335.

Di Luzio, G., Cusatis, G., 2009a. Hygro-thermo-chemical modeling of high performance concrete. i: Theory. Cement and Concrete composites 31 (5), 301–308.

Di Luzio, G., Cusatis, G., 2009b. Hygro-thermo-chemical modeling of high-performance concrete. ii: Numerical implementation, calibration, and validation. Cement and Concrete composites 31 (5), 309–324.

Di Luzio, G., Cusatis, G., 2013. Solidification–microprestress–microplane (smm) theory for concrete at early age: Theory, validation and application. International Journal of Solids and Structures 50 (6), 957–975.

Di Luzio, G., Ferrara, L., Krelani, V., 2018. Numerical modeling of mechanical regain due to self-healing in cement based composites. Cement and Concrete Composites 86, 190–205.

Diamond, S., 1983. Effects of microsilica (silica fume) on pore-solution chemistry of cement pastes. Journal of the American Ceramic Society 66 (5), C–82.

Fagerlund, G., 2009. Chemically bound water as measure of degree of hydration: method and potential errors. Division of Building Materials, Lund Institute of Technology.

Flatt, R. J., Scherer, G. W., Bullard, J. W., 2011. Why alite stops hydrating below 80% relative humidity. Cement and Concrete Research 41 (9), 987–992.

Garboczi, E., Bentz, D., 1992. Computer simulation of the diffusivity of cement-based materials. Journal of materials science 27 (8), 2083–2092.

Gawin, D., Pesavento, F., Schrefler, B. A., 2006a. Hygro-thermo-chemo-mechanical modelling of concrete at early ages and beyond. part i: hydration and hygro-thermal phenomena. International Journal for Numerical Methods in Engineering 67 (3), 299–331.

Gawin, D., Pesavento, F., Schrefler, B. A., 2006b. Hygro-thermo-chemo-mechanical modelling of concrete at early ages and beyond. part ii: shrinkage and creep of concrete. International Journal for Numerical Methods in Engineering 67 (3), 332–363.

Geiker, M., 1983. Studies of portland cement hydration by measurements of chemical shrinkage and a systematic evaluation of hydration curves by means of the dispersion model. Ph.D. thesis, Technical University of Denmark.

Hua, C., Acker, P., Ehrlacher, A., 1995. Analyses and models of the autogenous shrinkage of hardening cement paste: I. modelling at macroscopic scale. Cement and Concrete Research 25 (7), 1457–1468.

Jennings, H. M., Johnson, S. K., 1986. Simulation of microstructure development during the hydration of a cement compound. Journal of the American Ceramic Society 69 (11), 790–795.

Jensen, O. M., Hansen, P. F., 1999. Influence of temperature on autogenous deformation and relative humidity change in hardening cement paste. Cement and concrete research 29 (4), 567–575.

Jensen, O. M., Hansen, P. F., 2002. Water-entrained cement-based materials: Ii. experimental observations. Cement and Concrete Research 32 (6), 973–978.

Jiang, Z., Sun, Z., Wang, P., 2005. Autogenous relative humidity change and autogenous shrinkage of high-performance cement pastes. Cement and Concrete Research 35 (8), 1539–1545.

Kim, J.-K., Lee, C.-S., 1999. Moisture diffusion of concrete considering self-desiccation at early ages. Cement and Concrete Research 29 (12), 1921–1927.

Knudsen, T., 1982. Modeling hydration of portland cementthe effect of particle size distribution. In: Proceedings of the engineering foundation conference on characterization and performance prediction of cement

and concrete.

Koenders, E., Van Breugel, K., 1997. Numerical modelling of autogenous shrinkage of hardening cement paste. Cement and Concrete Research 27 (10), 1489–1499.

Legates, D. R., McCabe Jr, G. J., 1999. Evaluating the use of goodness-of-fit measures in hydrologic and hydroclimatic model validation. Water resources research 35 (1), 233–241.

Li, Y., Langan, B., Ward, M., 1996. The strength and microstructure of high-strength paste containing silica fume. Cement, Concrete and Aggregates 18 (2), 112–117.

Lin, F., Meyer, C., 2009. Hydration kinetics modeling of portland cement considering the effects of curing temperature and applied pressure. Cement and Concrete Research 39 (4), 255 – 265.

Livesey, P., Donnelly, A., Tomlinson, C., 1991. Measurement of the heat of hydration of cement. Cement and concrete composites 13 (3), 177–185.

Loukili, A., Khelidj, A., Richard, P., 1999. Hydration kinetics, change of relative humidity, and autogenous shrinkage of ultra-high-strength concrete. Cement and Concrete Research 29 (4), 577–584.

Lura, P., Guang, Y., Tanaka, K., Jensen, O. M., 2005. Micro-crack detection in high-performance cementitious materials. In: Fourth International Seminar on Self-desiccation and Its Importance in Concrete Technology. Lund University of Technology, pp. 165–178.

Lura, P., Jensen, O. M., van Breugel, K., 2003. Autogenous shrinkage in high-performance cement paste: An evaluation of basic mechanisms. Cement and concrete research 33 (2), 223–232.

Maekawa, K., Chaube, R., Kishi, T., 1999. Modeling of concrete performance: hydration, microstructure formation and mass transport. E and FN SPON, London 1.

Mainguy, M., Coussy, O., Eymard, R., 1999. Modélisation des transferts hydriques isothermes en milieu poreux. application au séchage des matériaux à base de ciment. No. OA 32.

Masoero, E., Cusatis, G., Di Luzio, G., 2018. C–s–h gel densification: The impact of the nanoscale on self-desiccation and sorption isotherms. Cement and Concrete Research 109, 103–119.

McGrath, P., Hooton, R., 1990. Self-desiccation of portland cement and silica fume modified mortars. Ceram. Trans. 16, 489–500.

Mitchell, D., Hinczak, I., Day, R., 1998. Interaction of silica fume with calcium hydroxide solutions and hydrated cement pastes. Cement and Concrete Research 28 (11), 1571–1584.

Molina, L., 1992. On predicting the influence of curing conditions on the degree of hydration. Cement och Betong Institututet.

Navi, P., Pignat, C., 1996. Simulation of cement hydration and the connectivity of the capillary pore space.

Advanced Cement Based Materials 4 (2), 58–67.

Nelder, J. A., Mead, R., 1965. A simplex method for function minimization. The computer journal 7 (4), 308–313.

Newman, E. S., 1950. A study of the determination of the heat of hydration of portland cement. Journal of Research of the National Bureau of Standards 45 (5).

Nilsson, L.-O., Mjörnell, K., 2005. A micro-model for self-desiccation in high performance concrete. In: Proceedings of the Fourth International Research Seminar, Gaithersburg, Maryland, USA.

Pan, Y., et al., 2017. Lattice modeling of early-age behavior of structural concrete. Materials 10 (3), 231.

Pathirage, M., Bentz, D. P., Di Luzio, G., Masoero, E., Cusatis, G., 2017. A multiscale framework for the prediction of concrete self-desiccation. Computational Modelling of Concrete Structures (G. Meschke, B. Pichler, and JG Rots, ed.), 203–207.

Pathirage, M., Bousikhane, F., DAmbrosia, M., Alnaggar, M., Cusatis, G., 2019. Effect of alkali silica reaction on the mechanical properties of aging mortar bars: Experiments and numerical modeling. International Journal of Damage Mechanics 28 (2), 291–322.

Persson, B., 1996. Hydration and strength of high performance concrete. Advanced Cement Based Materials 3 (3), 107–123.

Persson, B., Jun 1997. Self-desiccation and its importance in concrete technology. Materials and Structures 30 (5), 293–305.

Persson, B., Bentz, D., Fagerlund, G., 2005. Self-desiccation and its importance in concrete technology. In: Proceedings of the fourth international research seminar, Gaithersburg, Maryland, USA.

Pinson, M. B., Masoero, E., Bonnaud, P. A., Manzano, H., Ji, Q., Yip, S., Thomas, J. J., Bažant, M. Z., Van Vliet, K. J., Jennings, H. M., 2015. Hysteresis from multiscale porosity: modeling water sorption and shrinkage in cement paste. Physical Review Applied 3 (6), 064009.

Powers, T. C., Brownyard, T. L., 1946. Studies of the physical properties of hardened portland cement paste. In: Journal Proceedings. Vol. 43. pp. 101–132.

Principigallo, A., Lura, P., van Breugel, K., Levita, G., 2003. Early development of properties in a cement paste: A numerical and experimental study. Cement and Concrete Research 33 (7), 1013–1020.

Rahimi-Aghdam, S., Bažant, Z. P., 2018. Century-long durability of concrete structures: Expansiveness of hydration and chemo-mechanics of autogenous shrinkage and swelling. In: Computational Modelling of Concrete Structures. CRC Press, pp. 15–23.

Rahimi-Aghdam, S., Bažant, Z. P., Qomi, M. A., 2017. Cement hydration from hours to centuries controlled

by diffusion through barrier shells of csh. Journal of the Mechanics and Physics of Solids 99, 211–224.

Rasoolinejad, M., Rahimi-Aghdam, S., Bažant, Z. P., Mar 2019. Prediction of autogenous shrinkage in concrete from material composition or strength calibrated by a large database, as update to model b4. Materials and Structures 52 (2), 33.

Scrivener, K. L., 1986. The microstructure of anhydrous cement and its effect on hydration. MRS Online Proceedings Library Archive 85.

Sellevoid, E. J., 1987. Condensed silica fume in concrete. In: FIP/NB symposium on high strength concrete, Stavanger.

Sellevold, E., Justnes, H., 1992. High strength concrete binders part b: Nonevaporable water, self-desiccation and porosity of cement pastes with and without condensed silica fume. Fly Ash, Silica Fume, Slag, and Natural Pozzolans in Concrete. Fourth International ConferenceAmerican Concrete Institute 2 (SP-132).

Shvab, I., Brochard, L., Manzano, H., Masoero, E., 2017. Precipitation mechanisms of mesoporous nanoparticle aggregates: off-lattice, coarse-grained, kinetic simulations. Crystal Growth & Design 17 (3), 1316–1327.

Taylor, H. F., 1997. Cement chemistry. Thomas Telford.

Tazawa, E.-i., Miyazawa, S., Kasai, T., 1995. Chemical shrinkage and autogenous shrinkage of hydrating cement paste. Cement and concrete research 25 (2), 288–292.

Ulm, F.-J., Coussy, O., 1995. Modeling of thermochemomechanical couplings of concrete at early ages. Journal of engineering mechanics 121 (7), 785–794.

Van Breugel, K., 1995. Numerical simulation of hydration and microstructural development in hardening cement-based materials (i) theory. Cement and Concrete Research 25 (2), 319–331.

Wan, L., Wendner, R., Liang, B., Cusatis, G., 2016. Analysis of the behavior of ultra high performance concrete at early age. Cement and Concrete Composites 74, 120–135.

Xi, Y., Bažant, Z. P., Jennings, H. M., 1994. Moisture diffusion in cementitious materials adsorption isotherms. Advanced cement based materials 1 (6), 248–257.

Yang, Q.-b., Zhang, S.-q., 2004. Self-desiccation mechanism of high-performance concrete. Journal of Zhejiang University-Science A 5 (12), 1517–1523.

Ye, G., Van Breugel, K., Fraaij, A., 2003. Three-dimensional microstructure analysis of numerically simulated cementitious materials. Cement and Concrete Research 33 (2), 215–222.

Zhang, M.-H., Gjørv, O. E., 1991. Effect of silica fume on cement hydration in low porosity cement pastes. Cement and Concrete Research 21 (5), 800–808.